Application of multirate flowing fluid electric conductivity logging method to well DH-2, Tono Site, Japan

Christine Doughty,[1] Shinji Takeuchi,[2] Kenji Amano,[2] Michito Shimo,[3] and Chin-Fu Tsang[1]

Received 4 October 2004; revised 6 May 2005; accepted 17 June 2005; published 4 October 2005.

[1] In the flowing fluid electric conductivity (FEC) logging method, well bore fluid is replaced with deionized water, following which FEC profiles in the well bore are measured at a series of times while the well is pumped at a constant rate. Locations where fluid enters the well bore show peaks in the FEC logs, which are analyzed to infer inflow strengths and salinities of permeable features intersected by the borehole. In multirate flowing FEC logging, the flowing FEC logging method is repeated using two or more pumping rates. The results, coupled with those of a conventional well test over the entire borehole, enable the transmissivities and inherent pressure heads of permeable features to be determined. Multirate FEC logging is carried out on a deep borehole in fractured granitic rock using three different pumping rates. Results identify 19 hydraulically conducting fractures and indicate that transmissivity, pressure head, and salinity vary significantly among them. Using three pumping rates rather than the minimum number of two permits an internal consistency check on the analysis that provides a measure of the uncertainty of the results. Good comparisons against static FEC profiles and against independent chemical, geological, and hydrogeological data have further enhanced confidence in the results of the multirate flowing FEC logging method.

Citation: Doughty, C., S. Takeuchi, K. Amano, M. Shimo, and C.-F. Tsang (2005), Application of multirate flowing fluid electric conductivity logging method to well DH-2, Tono Site, Japan, *Water Resour. Res.*, *41*, W10401, doi:10.1029/2004WR003708.

1. Introduction

[2] Knowledge of the locations and hydraulic properties of conductive features is needed for understanding flow and transport through fractured rocks. Boreholes drilled deep into the rock are often employed to determine this information. Various downhole methods of studying fracture flow have been developed over the past few decades [*National Research Council*, 1996]. Coring and geophysical methods may be able to identify the fractures themselves, but they are unlikely to provide information on fracture flow properties. Straddle-packer pump-testing yields fracture flow properties but is very time consuming and expensive. Flow-logging techniques are an attractive alternative – they are sensitive to fracture flow and are efficient to deploy in the field. Several varieties of flow logging exist, including spinner surveys, heat pulse flowmeters [*Paillet and Pedler*, 1996; *Öhberg and Rouhiainen*, 2000], tracer dilution analysis [*Brainerd and Robbins*, 2004], and the flowing fluid electric conductivity (FEC) logging method, also known as hydrophysical logging, the technique employed in the present study. Since *Tsang et al.* [1990] introduced the method, it has been widely applied in deep wells down to 1500 m or more [*Kelley et al.*, 1991; *Guyonnet et al.*, 1993], in inclined boreholes drilled in the underground Grimsel Test Laboratory [*Marschall and Vomvoris*, 1995], and extensively in shallower wells down to about 100 m [*Evans et al.*, 1992; *Pedler et al.*, 1992; *Bauer and LoCoco*, 1996; *Paillet and Pedler*, 1996; *Karasaki et al.*, 2000]. Continued development of analytical and numerical data analysis techniques [*Löw et al.*, 1994; *Evans*, 1995; *Tsang and Doughty*, 2003; *Doughty and Tsang*, 2005] have broadened the range of applicability and enhanced the ease of use of the method.

[3] The flowing FEC logging method provides a means to determine hydrologic properties of fractures, fracture zones, or other permeable layers intersecting a borehole in saturated rock, by analyzing the time evolution of FEC logs obtained while the well is being pumped. Specifically, the method yields the locations, inflow strengths, and salinities of permeable features. If flowing FEC logging is repeated using different well pumping rates (a procedure known as multirate flowing FEC logging), then the transmissivities and inherent pressure heads of the different permeable features can also be determined [*Tsang and Doughty*, 2003]. Flowing FEC logging requires little or no specialized equipment or expertise, and may be carried out more quickly than most other methods, making it a valuable tool for efficient subsurface characterization.

[4] This paper presents the first field application of the multirate flowing FEC logging method, using data from the 500 m deep well DH-2 in the Tono area of Japan, and thus confirms the method proposed by *Tsang and Doughty* [2003]. Section 2 describes the method; section 3 shows

[1]Earth Sciences Division, Lawrence Berkeley National Laboratory, Berkeley, California, USA.
[2]Japan Nuclear Cycle Development Institute, Mizunami, Japan.
[3]Civil Engineering Research Institute, Technology Center, Taisei Corporation, Yokohama, Japan.

0043-1397/05/2004WR003708$09.00

the field test setup, measurement procedure, and data. Section 4 explains the analysis steps, and section 5 presents the results, including comparison with available independent data from the Tono site. Section 6 provides concluding remarks and recommendations.

2. Method

2.1. Data Collection

[5] In the flowing FEC logging method, the well bore water is first replaced by deionized water or, alternatively, by water of a constant salinity distinctly different from that of the formation water. This is done by passing deionized water down a tube to the bottom of the well bore at a low rate, while simultaneously pumping from the top of the well at the same rate. The goal is to completely replace the well bore water with deionized water without pushing any deionized water out into the rock formation. The FEC of the effluent is monitored throughout well bore water replacement, which continues until a low stable FEC value is reached. Next, the well is shut in and the deionized water tube is removed. Then the well is pumped from the top at a constant low flow rate Q_1 (e.g., several or tens of liters per minute), while an electric conductivity probe is lowered into the well bore to scan the FEC as a function of depth. This produces what is known as a flowing FEC log. With constant pumping conditions, a series of five or six FEC logs are typically obtained over a 1 or 2 day period. Optionally, the entire procedure may be repeated using a different pumping rate Q_2, typically half or double the original rate Q_1. Throughout the process, the water level in the well should be monitored.

2.2. Data Analysis

[6] At depth locations where water enters the well bore (inflow feed points), the FEC logs display peaks. These peaks grow with time and are skewed in the direction of water flow. By analyzing these logs as described below, it is possible to obtain the inflow rates and salinities of groundwater inflow from the individual feed points. Although locations where water leaves the well bore (outflow feed points) do not produce distinct peaks in the FEC logs, they can be identified by their impact on other peaks [*Doughty and Tsang*, 2005]. Recently the flowing FEC logging method has been extended to also determine the inherent pressure heads and transmissivities of the permeable features giving rise to the feed points, by performing flowing FEC logging using different pumping rates, a procedure called multirate flowing FEC logging [*Tsang and Doughty*, 2003].

[7] The numerical models BORE [*Hale and Tsang*, 1988] and the enhanced version BORE-II [*Doughty and Tsang*, 2000] calculate the time evolution of ion concentration (salinity) through the well bore by solving the one-dimensional advection-dispersion equation, given a pumping rate Q and a set of feed point locations z_i, strengths q_i, and salinities C_i (i.e., the forward problem). The governing equations for BORE-II are presented by *Doughty and Tsang* [2005]. Some analytical solutions are available for FEC profiles obtained from simple feed point configurations [e.g., *Drost et al.*, 1968; *Tsang et al.*, 1990], but BORE-II broadens the range of applicability of the analytical solutions by considering multiple inflow and outflow feed points, isolated and overlapping FEC peaks, early time and late time behavior, time-varying feed point strengths and salinities, as well as the interplay of advection and dispersion in the well bore.

[8] The general procedure for using BORE-II is to estimate feed point locations z_i by examining early time FEC profiles, then assign feed point properties (q_i and C_i) by trial and error until an acceptable match between modeled and observed FEC profiles is obtained (i.e., an inverse problem). If flowing FEC logs were only collected using one pumping rate Q, then the analysis ends here. However, if multiple sets of flowing FEC logs are available, the inverse procedure is repeated for each value of Q, with the inverse problems constrained by requiring that the same set of z_i and C_i values be used for each one.

[9] Assuming that two sets of flowing FEC logs were collected with pumping rates Q_1 and Q_2, and that the inflow rates from the transmissive fractures as evaluated by BORE-II are $q_i^{(1)}$ and $q_i^{(2)}$ respectively, then *Tsang and Doughty* [2003] showed that

$$\frac{T_i}{T_{tot}} = \frac{q_i^{(2)} - q_i^{(1)}}{Q_2 - Q_1} \tag{1}$$

and

$$\frac{P_i - P_{avg}}{P_{avg} - P_{wb}^{(1)}} = \frac{q_i^{(1)}/Q_1}{T_i/T_{tot}} - 1 \tag{2}$$

where T_i is the transmissivity of fracture i; $T_{tot} = \Sigma T_i$, which can be obtained by a normal well test over the entire borehole; P_i is the inherent pressure head of fracture i; $P_{avg} = \Sigma(T_i P_i)/T_{tot}$, which is the pressure in the well bore when it is shut in for an extended time; and $P_{wb}^{(1)}$ is the pressure drawdown in the well bore during the flowing FEC logging at $Q = Q_1$. The derivation of equations (1) and (2) assumes that the flow geometries within all the hydraulically conductive fractures intersecting the borehole are the same (e.g., all radial flow or all linear flow).

[10] The inherent pressure head P_i is the ambient or undisturbed pressure in a fracture or permeable layer that the borehole intersects. P_i is the value that would be measured under nonpumping conditions with packers inflated in the well bore on either side of the fracture to isolate the fracture for a substantial time period to attain steady state pressure conditions. To obtain P_i while the well is being pumped, pressure must be measured at a location beyond the influence of pumping; a distance that can be estimated as $1.5(tT_i/S_i)^{1/2}$ [*Cooper and Jacob*, 1946], where T_i/S_i is the hydraulic diffusivity of the fracture (transmissivity divided by storativity) and t is the time since pumping began.

[11] The pressure difference $P_i - P_{avg}$ provides a measure of the driving force for fluid flow between hydraulically conducting fractures and the well bore under nonpumping conditions. Note from the definition of P_{avg} above that if all the P_i values are the same, then $P_i = P_{avg}$, and thus there will be no internal well bore flow under nonpumping conditions. In this case, equation (2) shows that feed point strength q_i is proportional to fracture transmissivity T_i.

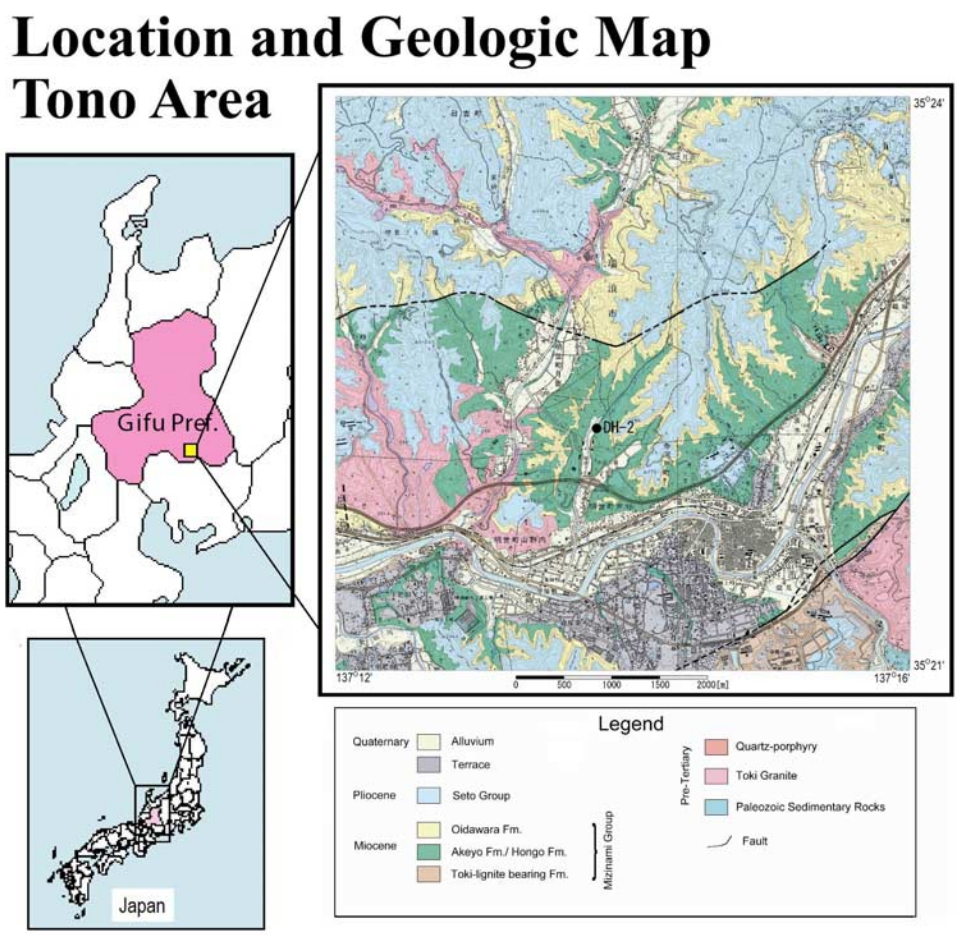

Figure 1. Site map of the Tono area, showing well DH-2.

[12] The ratios on the left-hand sides of equations (1) and (2) are the fundamental results of a multirate analysis. If T_{tot}, P_{avg}, and P_{wb} are also known (say from a conventional well test of the entire well section), then the T_i and P_i values themselves can be determined. Additionally, because T_i and P_i appear in ratios in equations (1) and (2), if one particular set of T_j and P_j are measured (say from a well test on a packed-off interval across fracture j), then all the additional T_i and P_i values can also be determined.

[13] *Tsang and Doughty* [2003] denoted the group on the left-hand side of equation (2) as the normalized pressure head difference, $(\Delta P)_n$. Note that the denominator of $(\Delta P)_n$ depends on Q_1 through $P_{wb}^{(1)}$. This Q dependence becomes inconvenient if several pairs of tests using different values of Q are to be compared. Hence both sides of equation (2) are multiplied by Q_1

$$\frac{P_i - P_{avg}}{P_{avg} - P_{wb}^{(1)}} Q_1 = \left(\frac{q_i^{(1)}/Q_1}{T_i/T_{tot}} - 1 \right) Q_1. \tag{3}$$

The ratio $Q_1/(P_{avg} - P_{wb}^{(1)})$ is known in the petroleum literature as the productivity index I, defined as the ratio of pumping rate to drawdown during a well test. I characterizes the well and the permeable formation it intersects but is independent of Q. Defining $(P_i - P_{avg}) = \Delta P_i$, equation (3) becomes

$$I\Delta P_i = \left(\frac{q_i^{(1)}/Q_1}{T_i/T_{tot}} - 1 \right) Q_1. \tag{4}$$

The quantity $I\Delta P_i$ provides a measure of inherent pressure head for the ith feed point that is independent of Q.

[14] To perform the multirate analysis, two sets of FEC logs at two pumping rates (at Q and $2Q$, for example) are all that is needed. However, if three sets of logs for three pumping rates, Q_1, Q_2 and Q_3 are available, then three sets of results can be obtained by analyzing three combinations of data: (Q_1 and Q_2), (Q_2 and Q_3) and (Q_3 and Q_1). This permits internal checking, a means to evaluate measurement errors, and an estimate on the confidence level of the analysis results.

3. Description of Tono Site, Testing Procedure, and Observed Data

[15] FEC logging was performed in well DH-2 very close to the Japan Nuclear Cycle Development Institute's MIU (Mizunami Underground Research Laboratory) site in the Tono area of Gifu Prefecture, Japan (Figure 1). The surface elevation at well DH-2 is 193 m, and the well itself is about

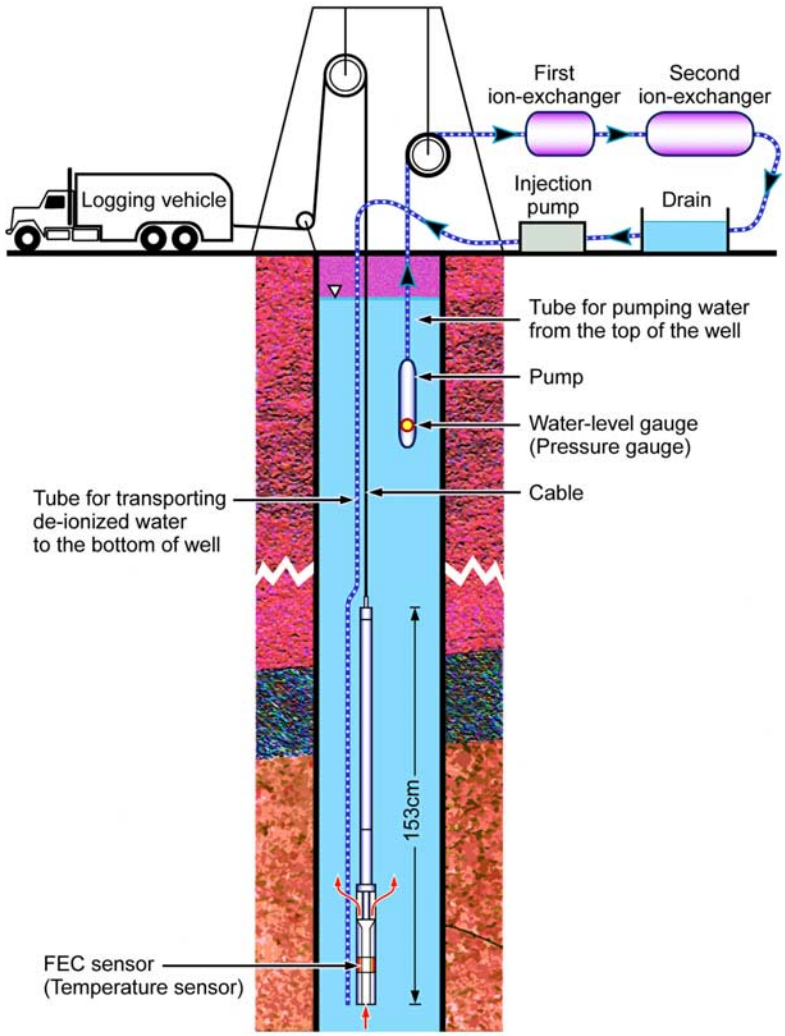

Figure 2. Field logging setup for replacement of well bore fluid by deionized water. During logging operations the setup is the same except that the tube for transporting deionized water to the bottom of the well is absent.

500 m deep. The upper 167 m of the well penetrates tertiary sedimentary rocks, which unconformably overly a medium-grained biotite granite of Cretaceous age that is weathered and highly fractured. Lithological logs from deeper wells in the Tono area suggest that at depths greater than several hundred meters, the granite becomes less fractured. The groundwater table is generally close to the ground surface in the Tono area. Well DH-2 is cased only over the sedimentary rock interval. The casing diameter is 118 mm, whereas the open-hole diameter is about 100 mm.

[16] The field instrumentation is shown in Figure 2. Three sets of FEC logs were obtained for three pumping rates Q: In test 1, Q_1 = 10 L/min (21–22 August 2002); in test 2, Q_2 = 20 L/min (22–23 August 2002); in test 3, Q_3 = 5 L/min (23–24 August 2002). For each test, a static FEC log was obtained prior to the start of pumping, and then seven FEC logs were measured at one-hour intervals, with pumping maintained at the constant rate. The complete field logging schedule for the three tests is shown in Table A1.

[17] Although the probe collects FEC data while moving both upward and downward through the well bore, only data collected while the probe is moving downward are useful for analysis, due to the configuration of the probe (Figure 2) and the pattern of fluid flow through and past it as it moves. The observed FEC data are shown in Figure 3.

[18] The water level in the well was also monitored over the period of the three tests. There is a great deal of uncertainty in the water level data from well DH-2, because of manipulation of borehole instrumentation between logging periods (see Table A1). The water level responses to the onset of pumping are qualitatively reasonable, with rapid initial declines followed by gradual achievement of plateaus and total water level changes on the order of 0.2–0.7 m. However, the overall water level uncertainty is on the order of 0.1 m, making it difficult to quantitatively interpret these water level changes. Table 1 shows the drawdowns with uncertainty levels for the three tests. Even more difficult is establishing a value for P_{avg}, the undisturbed pressure head in the well bore, which appears to decrease over time. Fortunately, the results of multirate flowing FEC logging do not depend on water level data; these are the left-hand sides of equations (1) and (4), the groups T_i/T_{tot} and $I\Delta P_i$, which describe the variability in transmissivity and inherent pressure head among conductive fractures inter-

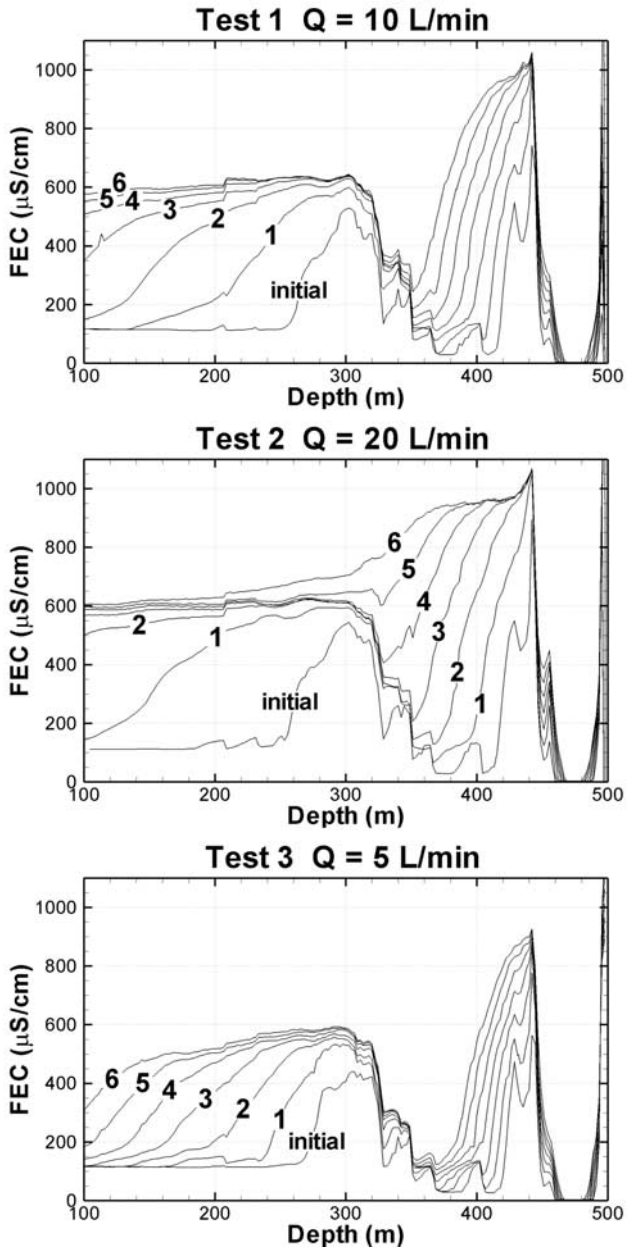

Figure 3. Observed FEC profiles for the three tests at Q = 10, 20, and 5 L/min. FEC values have been temperature corrected. The profile labeled "initial" is taken as soon as pumping commences. Numbers identify profile start time in hours.

sected by the borehole. The primary value of using water level data is to ensure that there are no unexpected observations not explainable by data uncertainties. To determine T_i and P_i values for comparison with other fracture characterization methods requires a separate, simple, conventional pumping test over the whole well bore, which is typically always conducted in a field study program.

[19] After the flowing FEC logging analysis was complete, FEC values of samples taken from different depth intervals in the borehole were obtained. These are used as a double-blind test of the FEC values obtained from flowing FEC logging for individual hydraulically conductive fractures. "Double-blind" means that the two sets of results are obtained from entirely different sets of measurements, both of which are analyzed without knowing the other results.

4. Analysis

4.1. Preliminary Data Processing

[20] FEC versus depth, and temperature T versus depth profiles were obtained for downward logging once prior to each test ("static profile") and seven times during each test (0, 1, 2, 3, 4, 5, 6 hours after pumping began). The cable speed of the probe, v, is assumed to be constant and is inferred from starting and ending times of the logging run and the distance logged. A time is assigned to each (FEC, z) data pair based on $t = t_{start} + (z - z_{start})/v$.

4.1.1. Temperature Correction

[21] Temperature increases with depth from about 23°C to 27°C over the depth interval of interest between 100 m and 500 m below the ground surface, whereas BORE-II considers FEC at a uniform temperature of 20°C. FEC data collected at various temperatures may be converted to 20°C conditions using the formula [*Schlumberger*, 1984]

$$\mathrm{FEC}(20^\circ\mathrm{C}) = \mathrm{FEC}(T)/[1 + S(T - 20^\circ\mathrm{C})], \quad \text{with } S = 0.024^\circ\mathrm{C}^{-1}. \tag{5}$$

4.1.2. FEC/Salinity Relationship

[22] The FEC/salinity relationship [*Hale and Tsang*, 1988]

$$\mathrm{FEC} = 1870C - 40C^2 \tag{6}$$

is used to convert feed point salinities C (g/L) to FEC values (μS/cm) within BORE-II and to set up initial salinity conditions for BORE-II.

4.1.3. Choice of Initial Conditions

[23] Figure 4 shows two early time FEC profiles for each of the three tests. The FEC profiles labeled "static" were obtained under nonpumping conditions, about two hours after the deionization process ended, and about one-half hour before pumping began (see Table A1). The presence of peaks in the static FEC profiles indicates that even when the well is not pumped, internal flow occurs in the well bore, driven by different pressure heads at different depths. Theoretically, one could use the static profiles as initial conditions, model the internal flow for one-half hour, use time-dependent feed point strengths to represent the onset of pumping, and model the remaining six hours of pumping. However, it is particularly difficult to infer feed point properties from FEC profiles arising from internal flow, because there is as much invisible outflow as visible inflow. Therefore we opt to begin modeling at the onset of pumping, using as initial conditions the FEC profiles labeled "flowing" in Figure 4, which were obtained just after pumping commenced. A minor complication is that

Table 1. Estimate of Drawdown Data for the Three Tests

Test	Pump Rate Q, L/min	Pressure Drawdown, m
1	10	0.25 ± 0.05
2	20	0.7 ± 0.10
3	5	0.2 ± 0.12

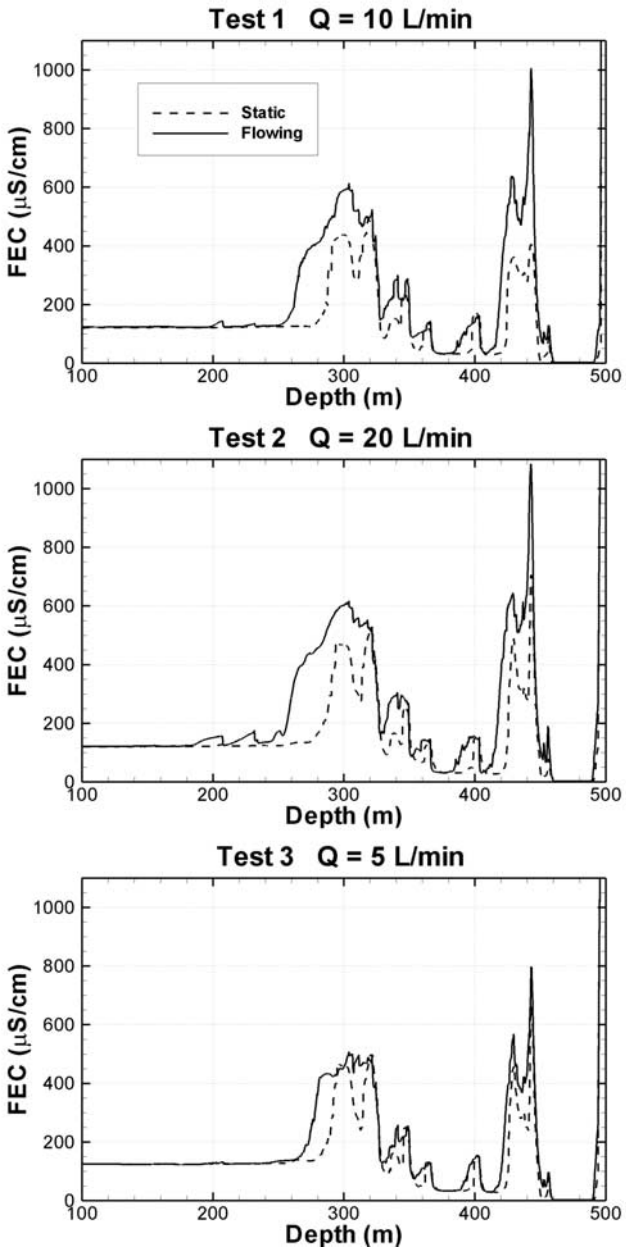

Figure 4. Early time observed FEC data for the three tests. The line labeled "static" is the nonpumping FEC profile collected after the well bore water has been replaced by deionized water and before pumping begins. The line labeled "flowing" represents the first FEC profile measured just after pumping started (after about 4–7 min of pumping).

BORE-II does not expect initial conditions to have a time variation such as FEC profiles have (e.g., the beginning and ending times of this log are 8:35 am and 8:51 am for test 3). So the entire "flowing" profile is assigned an intermediate time (e.g., 8:43 for test 3), which is used as the initial condition for BORE-II.

[24] At the completion of the multirate flowing FEC log analysis of tests 1, 2, and 3, we will be in a better position to analyze the static profiles, because determining T_i/T_{tot} and $I\Delta P_i$ for all the feed points using equations (1) and (4) permits prediction of q_i when $Q = 0$. This procedure is carried out in section 5.2.

4.2. Test 3 BORE-II Analysis

[25] Analysis begins with test 3, $Q = 5$ L/min, because the lowest pumping rate enables individual feed points to be identified most readily. The steps in the matching process are as follows: (1) Locate 20 feed points by eye from initial FEC profile. (2) Categorize feed points as tiny (8 of 20), small (5 of 20), medium (6 of 20), or large (1 of 20). (3) Ignore tiny feed points. (4) Assign q_i roughly for small, medium, and large feed points with $\Sigma q_i = Q = 5$ L/min. (5) Assign the same C_i (denoted C_1) to all the feed points (with C_1 chosen arbitrarily). (6) Run BORE-II. (7) Correct the order of magnitude of C_1 by visual inspection of the modeled and observed FEC profiles and run BORE-II again. (8) Match individual peaks: vary C_i and q_i values by trial and error, always keeping $\Sigma q_i = Q$; run BORE-II; compare modeled and observed FEC profiles; repeat. Add tiny feed points as needed.

[26] The best match to the observed FEC profiles is shown in Figure 5a, followed by plots showing the feed point strengths (Figure 5b) and salinities (Figure 5c) that produce the match. The ticks in Figure 5a identify 14 feed point locations, and the semicircle shows where a well bore diameter change is inferred (discussed below). Overall, the match between model and observed FEC profiles shown in Figure 5a is considered quite good.

4.2.1. Well Bore Diameter Change at 170 m Depth

[27] The diameter of well DH-2 changes at about 170 m depth, where the well casing ends. The larger well bore diameter above 170 m provides a larger cross-sectional area for flow, so for a constant volumetric flow rate, the velocity at which FEC peaks move up the well bore decreases. Assuming that well bore fluid is thoroughly mixed over the well bore cross-sectional area, a simple mass balance calculation shows that when a peak reaches 170 m its upward velocity decreases by a factor A_1/A_2, where A_1 and A_2 are the well bore cross-sectional areas below and above 170 m, respectively. BORE II assumes a constant diameter well bore, but the increase in diameter can be mimicked by assigning an outflow feed point at 170 m with strength chosen such that when flow up the well bore below the outflow point is Q, flow up the well bore above the outflow point will be Q (A_1/A_2). That is, $Q_{out} = Q(1 - A_1/A_2)$. The salinity of the outflow point will vary with time, always equaling the salinity in the well bore at the outflow point depth.

[28] Figure 6 shows the shallow FEC profiles predicted for test 3 for casing diameters of 100, 119, or 127 mm, with an outflow feed point of strength $Q\,(1 - A_1/A_2)$ at 170 m. A 100 mm casing means that the well bore diameter is constant over the entire well length, so $A_1 = A_2$ and outflow at 170 m is zero; 127 mm is the value originally reported for the casing diameter. Neither value produces a good fit to the observed FEC profiles above 170 m depth, but the model results do bracket the data. By trial and error, 118–119 mm casing diameters were found to yield good fits to the observed FEC profiles. Therefore a 119 mm casing is assumed for all BORE II simulations, by assigning an outflow point with strength $0.3Q$ at 170 m depth.

[29] Subsequent to the analysis of well DH-2 flowing FEC logs, a caliper log of well DH-2 was obtained

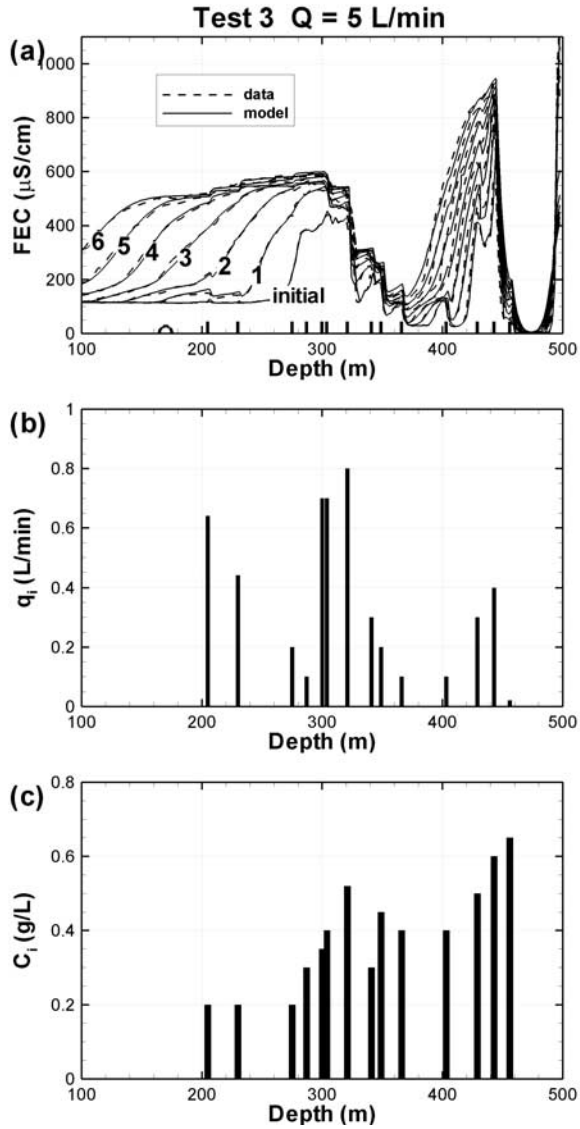

Figure 5. Independent analysis of test 3 (Q = 5 L/min): (a) Best FEC match between model and data, (b) inflow rates of feed points, and (c) salinity of feed points.

(Figure 7). The log includes the bottom 2 m of the cased interval, and shows the casing inner diameter to be about 118 mm, equal to the value inferred from BORE II simulations. This finding demonstrates that matching FEC data with simulation results can unveil a small systematic difference in well bore diameter, and illustrates how a BORE II analysis may be used to check the consistency of information provided about the system. Figure 7 also verifies that assuming the uncased portion of the well bore to have a uniform diameter is reasonable. Small variations in diameter do exist, and in fact can be correlated to feed points at 320, 430, and 455 m (see Figure 5), but the diameter changes average out to zero within very short depth ranges, enabling a reasonable fit to the observed FEC profiles under the assumption of a uniform well bore diameter. The study illustrates the fact that the results of the flowing FEC logging method are not sensitive to small local variations of well bore radius (see also *Doughty and Tsang* [2005], which discusses the effect of nonuniform

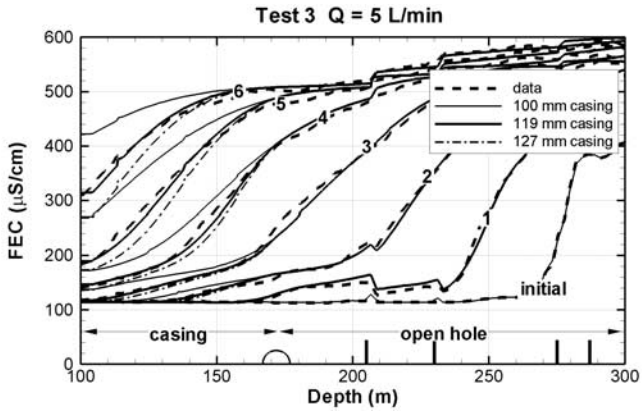

Figure 6. Sensitivity study showing effect of well bore diameter change at 170 m on FEC profiles.

well bore radius on various characterization methods for fracture flow).

4.2.2. Sensitivity to Dispersion Coefficient

[30] The constant dispersion coefficient used for BORE-II, $D_0 = 0.001$ m^2/s, was determined by trial and error along with the feed point properties. The fact that D_0 is orders of magnitude greater than typical molecular diffusion coefficients suggests that there is significant dispersion occurring in the well bore. This is expected given the continuous motion of the probe up and down the well bore. Moreover, a Reynolds number calculation indicates that even with no probe motion, well bore flow becomes turbulent for $Q >$ 10 L/min, providing another source of enhanced dispersion.

[31] For Q = 5 L/min and a 100 mm diameter well bore, velocity is 0.01 m/s. Dispersion coefficient can be converted to dispersivity by dividing by velocity, yielding a dispersivity of 0.1 m, equal to the well bore diameter. This is consistent with the a priori assumption that concentration is constant over the well bore cross-sectional area, which enables use of the one-dimensional advection-dispersion

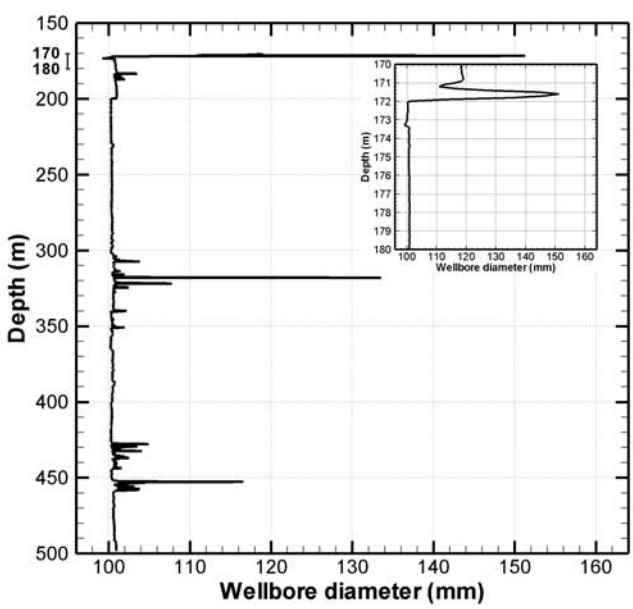

Figure 7. Caliper log for well DH-2. Inset shows depth interval around bottom of casing.

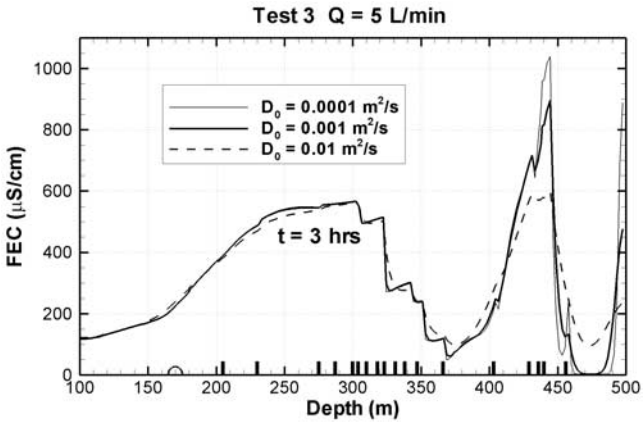

Figure 8. Sensitivity study showing effect of dispersivity on an FEC profile.

equation. Figure 8 illustrates the effect on the FEC profile of increasing and decreasing dispersion coefficient by a factor of 10. The biggest change occurs around z = 430 m, where several closely spaced feed points with small q_i and large C_i form an isolated peak. Above z = 320 m, multiple feed points with large q_i create a single wide peak, making the profile advection-dominated and nearly independent of D_0.

4.2.3. Nonuniqueness of Parameters Inferred From Test 3 Match

[32] When looking at a match between observed and modeled FEC profiles, it is necessary to consider how well constrained the corresponding feed point parameters are. For test 3, there may be other combinations of flow rate and salinity that would yield a comparably good match, because the area under an FEC peak is proportional to the product q_iC_i, making q_i and C_i inversely related. However, one general conclusion can be made: the C_i values for the different feed points cannot all be the same. At the depth of 443 m, C must be relatively large so that q can be relatively small, in order for the peak to show little skewing with time. At the depths of 275, 230 and 205 m, C must be progressively smaller to get the "stepping down" pattern in the FEC profile.

4.3. Test 2 BORE-II Analysis

[33] Test 2 is analyzed next, because with a pumping rate of Q = 20 L/min, it has the largest pumping rate of any test, and produces the most different conditions from test 3, which has the smallest pumping rate. To start the analysis, the C_i and q_i values are varied to best match the observed FEC profiles, without taking into consideration any of the results of the test 3 analysis. Four additional feed points are added. The resulting FEC profiles and feed point properties are shown in Figure 9. For depths greater than 240 m, the match is comparably good to that for test 3, whereas above 240 m it is not quite as good.

[34] Next, the C_i values for tests 3 and 2 (Figures 5c and 9c) are compared. Both tests yield C_i values that generally increase with depth from 0.2 g/L to 0.8 g/L, but individual C_i values at some depths differ between tests. Because changing pumping rate should change q_i values but not C_i values between tests, tests 3 and 2 are reanalyzed using same set of C_i values for each test. One additional feed point is added, and several feed point depths are also adjusted slightly from the analysis of test 3, because test 2, with its higher Q, gives a better indication of locations for fractures with small q_i. Requiring that the models for both tests 3 and 2 use the same C_i values slightly worsens the shallow (z < 240 m) match for test 3 compared to the previous individual test analysis, suggesting that feed points with z < 240 m are not as well characterized as deeper feed points.

4.4. Test 1 BORE-II Analysis

[35] To determine the feed point strengths for test 1, $q_i^{(1)}$, equation (1) is applied, considering T_i/T_{tot} to be known from Q_2, Q_3, and the $q_i^{(2)}$, and $q_i^{(3)}$ values obtained from the tests 2 and 3 analyses. Solving for $q_i^{(1)}$ yields

$$q_i^{(1)} = q_i^{(2)} - \frac{T_i}{T_{tot}}(Q_2 - Q_1) \tag{7}$$

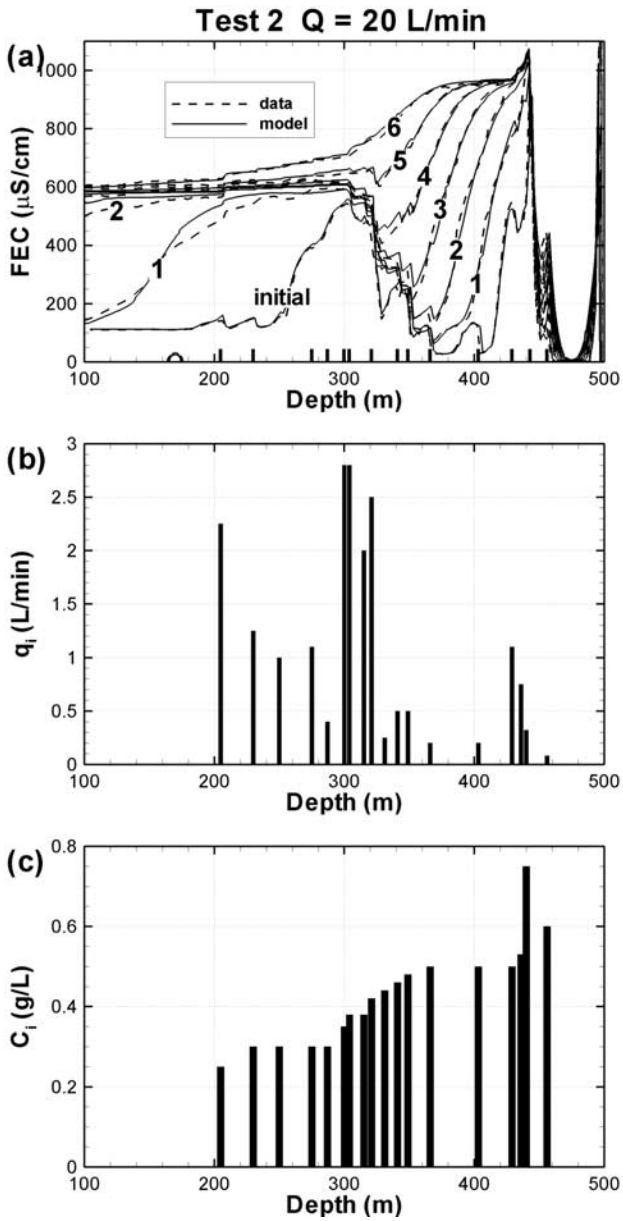

Figure 9. Independent analysis of test 2 (Q = 20 L/min): (a) best FEC match between model and data, (b) inflow rates of feed points, and (c) salinity of feed points.

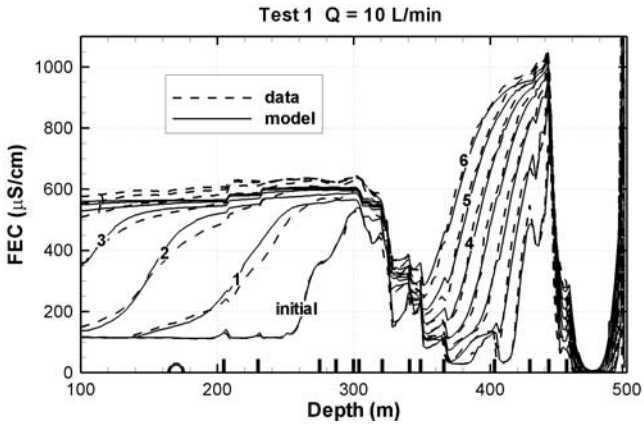

Figure 10. Observed and modeled FEC profiles for test 1 (Q = 10 L/min) for a model using feed point strengths and salinities inferred from the combined analysis of tests 2 and 3. No fitting to test 1 data was done.

[36] The resulting FEC profiles are shown in Figure 10 along with the corresponding observed data. The deeper portion of the profile (z > 320 m) shows a good match, whereas in the shallower portion, the model underpredicts the observed FEC values. Figure 10 shows a type of validation test in that it uses results from analyses of tests 2 and 3 to predict the results of test 1 and compare them to test 1 field data. Overall, the agreement is considered acceptable, as there is no fitting involved. Recall that both the individual test 2 analysis (Figure 9a) and the combined analysis for tests 2 and 3 (results not shown) produce better matches for the deeper half of the profile than for the shallower half, suggesting that the deeper half of the interval is better characterized. Hence it is not surprising that the match for test 1 is also better for the deeper half.

4.5. Combined BORE-II Analysis

[37] The q_i and C_i values for all three tests are modified together to simultaneously match all the FEC profiles, using a single set of C_i values. The best match FEC profiles are shown in Figure 11, and Figure 12 shows the feed point strengths and salinities used to produce the match. For z > 320 m, no feed point changes from the previous models are needed, as the matches for all three tests were already good. For z < 320 m, the updated match for test 1 is greatly improved (compare Figure 10), whereas the matches for tests 2 and 3 are little changed from the previous models.

[38] Figure 11 shows that the skewing of the peaks up the well bore, which constrains q_i, is most apparent for the small Q of test 3, whereas the achievement of FEC plateaus, which constrains C_i. is most apparent for the large Q of test 2. Thus the inherent nonuniqueness between q_i and C_i discussed at the end of section 4.2 can be ameliorated by repeating logging using different values of Q.

[39] Studies with synthetic flowing FEC data (where the true values of q_i and C_i are known) have been used to investigate nonuniqueness. When an analysis of closely spaced peaks is conducted using only one value of Q, erroneous assumptions for C_i can be concealed by choosing q_i such that the product q_iC_i for each peak and the sum Σq_i over all peaks are correct, yielding a reasonable fit to the FEC profiles. However, when multiple Q values are used, it is much less likely (although not impossible) that reasonable fits to all profiles can be obtained with erroneous C_i values.

5. Multirate Results and Consistency Tests

5.1. Comparing Pairs of Tests With Different Q

[40] The three tests can be compared two at a time to investigate individual fracture transmissivities and inherent pressure heads using equations (1) and (4). Because T_{tot}, P_{avg}, and P_{wb} are unknown, T_i and P_i values cannot be explicitly determined, but the groups T_i/T_{tot} and $I\Delta P_i$ provide valuable information on the flow behavior of the fractures relative to one another (Figure 13).

[41] The combined display of Figure 13 serves three purposes. First, it incorporates all the data collected during

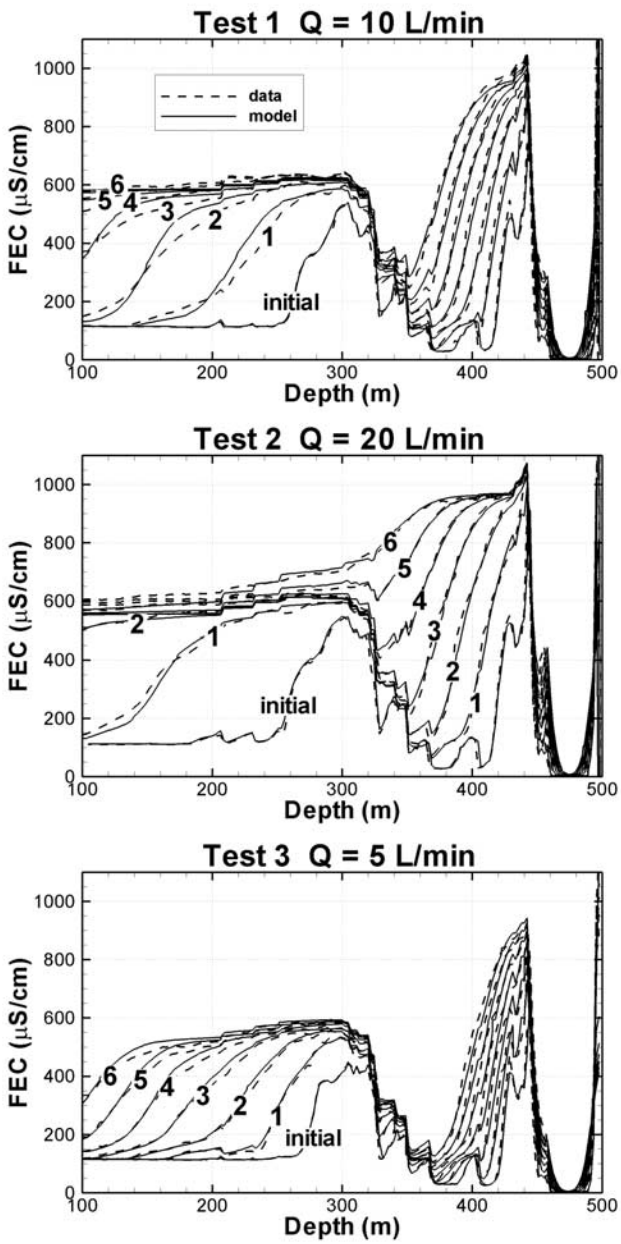

Figure 11. Best match FEC profiles for a combined analysis of tests 1, 2, and 3 using the same feed point salinities for each test.

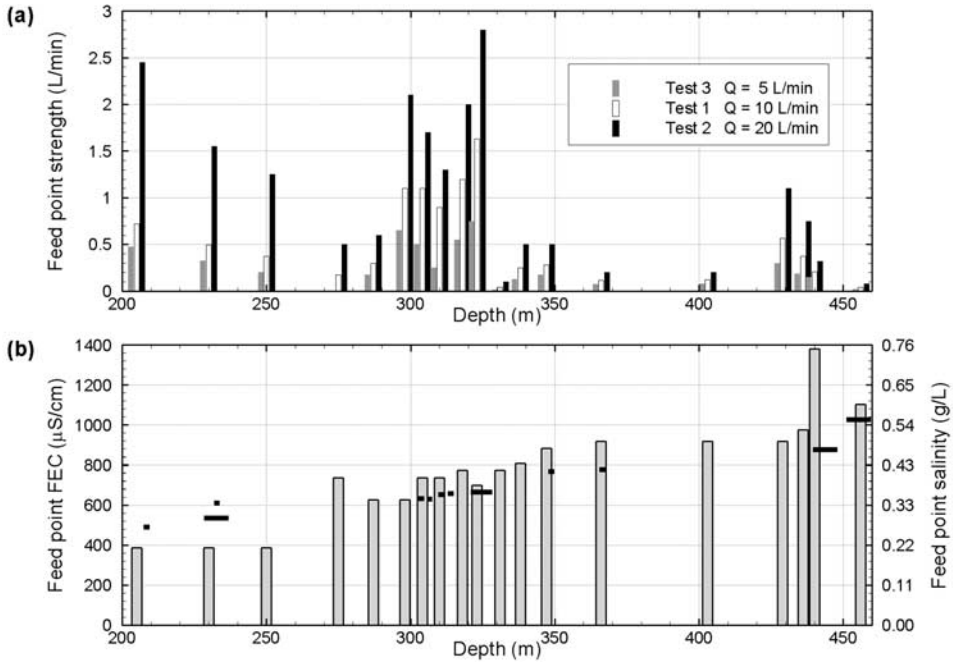

Figure 12. (a) Feed point strengths for all three tests and (b) FEC or salinity of feed points (same for all tests). The solid line segments show independent information on FEC values in isolated well bore intervals (section 5.3), which was not used in the present analysis.

the three tests to provide the best estimate for the transmissivity and inherent pressure head of each hydraulically conductive fracture intersecting the borehole. Second, the agreement between different pairs of tests supplies a measure of confidence in the results – the better the agreement, the more confidence. Third, when doing further analyses of the poorly agreeing feed points, trial choices of q_i can be tailored to minimize the discrepancy between the different test pairs.

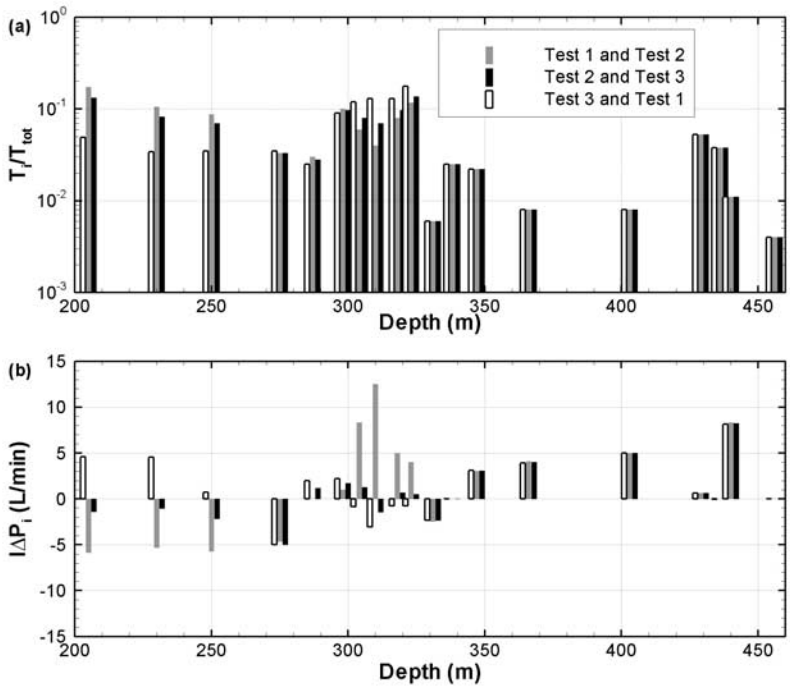

Figure 13. Results obtained for three combinations of the three tests: (a) feed point transmissivities divided by total transmissivity (from equation (1)) and (b) productivity index times pressure head difference (from equation (4)).

Table 2. Information on Hydraulically Conducting Fractures Based on Combined Analysis of Tests 2 and 3

Depth, m	$q_i^{(2)}$, L/min	$q_i^{(3)}$, L/min	$\frac{T_i}{T_{tot}}$ [a]	$\frac{T_i}{T_{bar}}$	$I\Delta P_i$, [b] L/min
205	2.45	0.473	0.132	2.504	−1.42
230	1.55	0.325	0.082	1.552	−1.02
250	1.25	0.200	0.070	1.330	−2.14
275	0.50	0.000	0.033	0.633	−5.00
287	0.60	0.175	0.028	0.538	1.18
298	2.10	0.650	0.097	1.837	1.72
304	1.70	0.500	0.080	1.520	1.26
310	1.30	0.250	0.070	1.330	−1.42
318	2.00	0.550	0.097	1.837	0.68
323	2.80	0.750	0.137	2.597	0.48
331	0.10	0.015	0.006	0.108	−2.36
338	0.50	0.125	0.025	0.475	0.00
347	0.50	0.175	0.022	0.412	3.08
366	0.20	0.075	0.008	0.158	4.00
403	0.20	0.080	0.008	0.152	5.00
429	1.10	0.300	0.053	1.013	0.62
436	0.75	0.187	0.038	0.713	−0.02
440	0.32	0.150	0.011	0.215	8.24
456	0.08	0.020	0.004	0.076	0.00
Entire well bore	20	5	1	1/19	

[a]Figure 13a.
[b]Figure 13b.

[42] For depths greater than 325 m and for depths between 270 m and 300 m, the agreement is excellent for both transmissivity and inherent pressure head. Elsewhere, the agreement for transmissivity is good (well within an order of magnitude), but could certainly be better, and the agreement for inherent pressure head is less than satisfactory, pointing out where further analysis efforts should focus. Note that for both quantities, the test 1/test 2 analysis and the test 2/test 3 analysis agree better with each other than with the test 3/test 1 analysis. Hence, when there is a contradiction between results, less credence is given to the test 3/test 1 results. On the basis of the test 1/test 2 and test2/test3 results, there is a trend of increasing inherent pressure head with depth. Not surprisingly, the least certain results are for depths between 300 and 325 m, where $I(\Delta P)_i$ changes sign.

[43] Overall, the test 2/test 3 results are considered to be the most reliable, in part because for feed points with large discrepancies between the three test pairs, they provide the middle value. Moreover, they do not rely on test 1 results, which as the first test conducted, may give less dependable results. Table 2 summarizes the properties of the 19 identified hydraulically conductive fractures as obtained from the combined tests 2/test 3 analysis. In Table 2, T_{tot} and T_{bar} are the total transmissivity of the well bore interval from 200 to 480 m and the mean transmissivity averaged over the 19 fractures, respectively.

5.2. Static Profiles

[44] Recall that the pressure head difference $(P_i - P_{avg})$ provides a measure of the driving force for fluid flow between hydraulically conducting fractures and the well bore under nonpumping conditions. Figure 13b presents $I(P_i - P_{avg}) = I\Delta P_i$ for the 19 hydraulically conductive fractures obtained by the analysis of test 2 and test 3. Fractures at depths 287, 298, 304, 318, 323, 347, 366, 403, 429 and 440 m have positive values of $I\Delta P_i$, meaning they have pressure heads above the mean shut-in well bore pressure P_{avg}. This means that at $Q = 0$, with no pumping of the well bore, there will be internal flow in the well bore, with inflows coming in from these fractures. Examination of the FEC profiles in the well bore before pumping starts for all three tests (see Figure 4 curves labeled "static"), shows that the FEC peaks occur at depths of about 300, 320, 340, 350, 365, 405, 430, and 440 m, exhibiting very good correspondence to the high-P_i feed points.

[45] This comparison can be quantified by using BORE II to simulate the nonpumping period. When $Q = 0$, equation (7) to determine feed point strength simplifies to:

$$q_i^{(0)} = q_i^{(2)} - \frac{T_i}{T_{tot}} Q_2 \tag{8}$$

Using equation (8) and the values from Table 2 to determine $q_i^{(0)}$, and taking feed point salinity values from Figure 12b, BORE II simulates the 2 hour period between the time when the deionizing equipment was removed from the well and the time when the "static" (nonpumping) profile was logged for test 3. Results are shown in Figure 14. Considering that this is a double-blind test, the agreement with the main peaks in the static profile is remarkably good. This provides additional confidence on the correctness of the test 2/test 3 results. Note that if a nonpumping simulation had been done using the high-P_i feed points predicted by the test 3/test 1 pair, the agreement would not have been nearly as good (e.g., there would have been static peaks predicted at depths of 205 and 230 m).

5.3. Comparison to Other Data

[46] Here, results of flowing FEC logging are compared with other data collected from well DH-2. None of these data were examined until after the BORE II analyses had been completed. Details on how the other data were collected appear in a companion paper that describes the entire suite of hydrogeologic testing performed at the Tono Site (S. Takeuchi et al., Integrated hydrogeologic investigation in a fractured rock, manuscript in preparation, 2005).

5.3.1. C_i From Measurements on Water Samples

[47] Measured FEC values from short zones of the well bore were obtained after the BORE II analyses were complete; they are shown as black line segments in

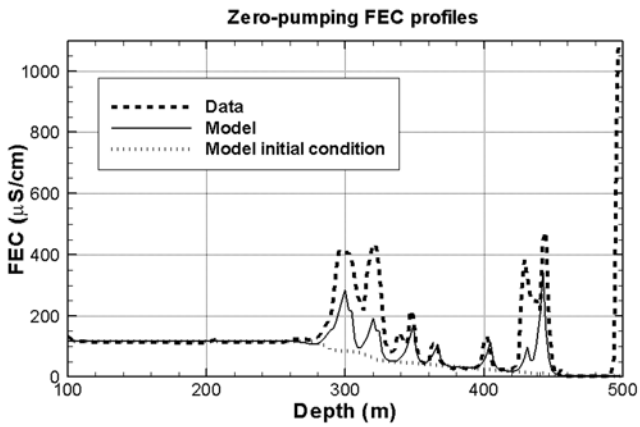

Figure 14. Modeled and observed FEC peaks produced by internal well bore flow prior to test 3.

Figure 12b. The model reproduces the general trend of increasing salinity with depth correctly, but the model C_i values are generally higher. This perhaps can be expected, since the model results give FEC of the fracture water, but water sampling may include well bore water mixed with it, depending on the sampling method and conditions.

5.3.2. Lithology

[48] The lithostratigraphical column (Figure 15), taken from core obtained during drilling, indicates that the majority of the well bore interval used for flowing FEC logging and the locations of all feed points, lie within the Toki granite. The two fault zones noted within the granite correspond to feed point depths identified from FEC peaks (also shown in Figure 15), suggesting that they have hydrological significance.

5.3.3. Fracture Density

[49] The fracture density profile (Figure 15), obtained from borehole televiewer data, shows numerous fractures distributed over almost the entire borehole length. Some of the depths showing intense fracturing can be correlated to feed point locations, including depths of 205, 230, 304, 310, 318, 323, 347, 429, 436, 440 and 456 m, which are lithologically identified as fractured zones. Additionally, Figure 15 shows that the depth range from 360 to 400 m has a low fracture density, and FEC logging identified only two weak feed points within this range (Figure 12). However, the correlation is not perfect. For example, the depth ranges of 170–200 m and 250–300 m appear quite similar in the fracture density data. In contrast, FEC logging produces no feed points at all within the 170–200 m range, but several moderate-strength feed points in the 250–300 m range (Figure 12). These observations corroborate the notion that fractures with apparently similar geometric properties such as aperture, spacing, and orientation can vary tremendously in their transmissivity, and visual identification of the fractures themselves is not generally sufficient to predict transmissivity.

5.3.4. Alteration

[50] Weathering and alteration (Figure 15) are typically indicators of large fluid flow, and the two depth intervals within the granite showing the most alteration, 315–320 and 427–470 m, correspond to the most significant inflow zones (Figure 12a).

5.3.5. Transmissivity

[51] Transmissivity measurements (Figure 15), obtained from slug tests and pulse tests on packed-off intervals, targeted mainly the water-conducting fractures, and indicate that all but one of these fractures have a transmissivity in the range from about 10^{-6} to 10^{-4} m^2/s. The transmissivities shown in Figure 13a vary by a factor of about 40, consistent with this range. Every transmissivity measurement in Figure 15 corresponds to a feed point, and generally, the depths with the highest transmissivities (205, 230, 300–320, 430) correspond to the feed points with the highest T_i values (Figure 13a).

[52] Quantitative comparison of individual T_i values from flowing FEC logging with packer test T values is not possible without knowledge of P_{avg} and P_{wb}, but such comparisons may not be especially valuable in any event, for the following reason. During a packer test, water is pumped from just one interval of a well bore, the packed-off interval that intersects a targeted fracture. Water flowing into the well bore originates not only in this one fracture, but in the network of fractures connected to it. Thus the T value determined from the packer test is representative of the connected fracture network rather than just one fracture. When the packers are moved to an adjacent interval, contributions of fractures directly next to the borehole change, but at a short distance away many of the same fractures contribute to the flow. Thus, if one adds up the T values obtained during a series of packer tests along adjacent intervals, one will overestimate the total transmissivity of the borehole. In contrast, in flowing FEC logging, water flows into the well bore simultaneously from fractures all along the well bore. Thus the sum of the individual feed point transmissivities does equal the total transmissivity.

[53] On the basis of correlation with results from geological and geophysical investigations, 15 of the 19 feed points identified with flowing FEC logging correspond to major fractures (or fracture zones). For example, borehole radar logging was carried out with a directional radar antenna, with a central frequency of 60 MHz. F-K filtering was applied to the raw data to identify reflectors more effectively and precisely. Figure 16 shows mapped reflectors identified with the directional borehole radar technique. These major fractures dip steeply to moderately, and are either E-W trending, N-S trending, or ENE-WSW trending.

6. Discussion and Conclusions

[54] Performing the flowing FEC logging method at different pumping rates has enabled us to not only estimate inflow strengths and salinities of hydraulically conductive fractures intersecting well DH-2, but also to compare their transmissivities and inherent pressure heads. Moreover, using three pumping rates provides a consistency check on the analysis that supplies a measure of the uncertainty of the results. Comparisons against static FEC profiles and independent chemical, geological, and hydrogeological data provide further checks on the validity of the multirate flowing FEC logging method results.

[55] In particular, comparing the flowing FEC logging results from each test pair with each other and with independent data makes it clear that the match at shallow inflow points can be improved. One possible approach would be to increase C_i for shallow feed points according to values from water sampling (Figure 12b). We expect that all shallow FEC profile matches and consistency among results for different test pairs would be greatly improved by such considerations.

[56] In general, using a variety of techniques for hydrogeological characterization is preferable to using just one. The strengths and weaknesses of different methods complement each other, providing a much more reliable picture of the subsurface, particularly for heterogeneous or fractured media. The primary purpose for performing flowing FEC logging without making use of other data sources was to demonstrate and highlight its capabilities to efficiently determine flow rate, salinity, transmissivity, and inherent pressure head of hydraulically conductive fractures. Having done so, we are now in a good position to integrate all available data to arrive at a better understanding of the hydraulics of the fractured rock.

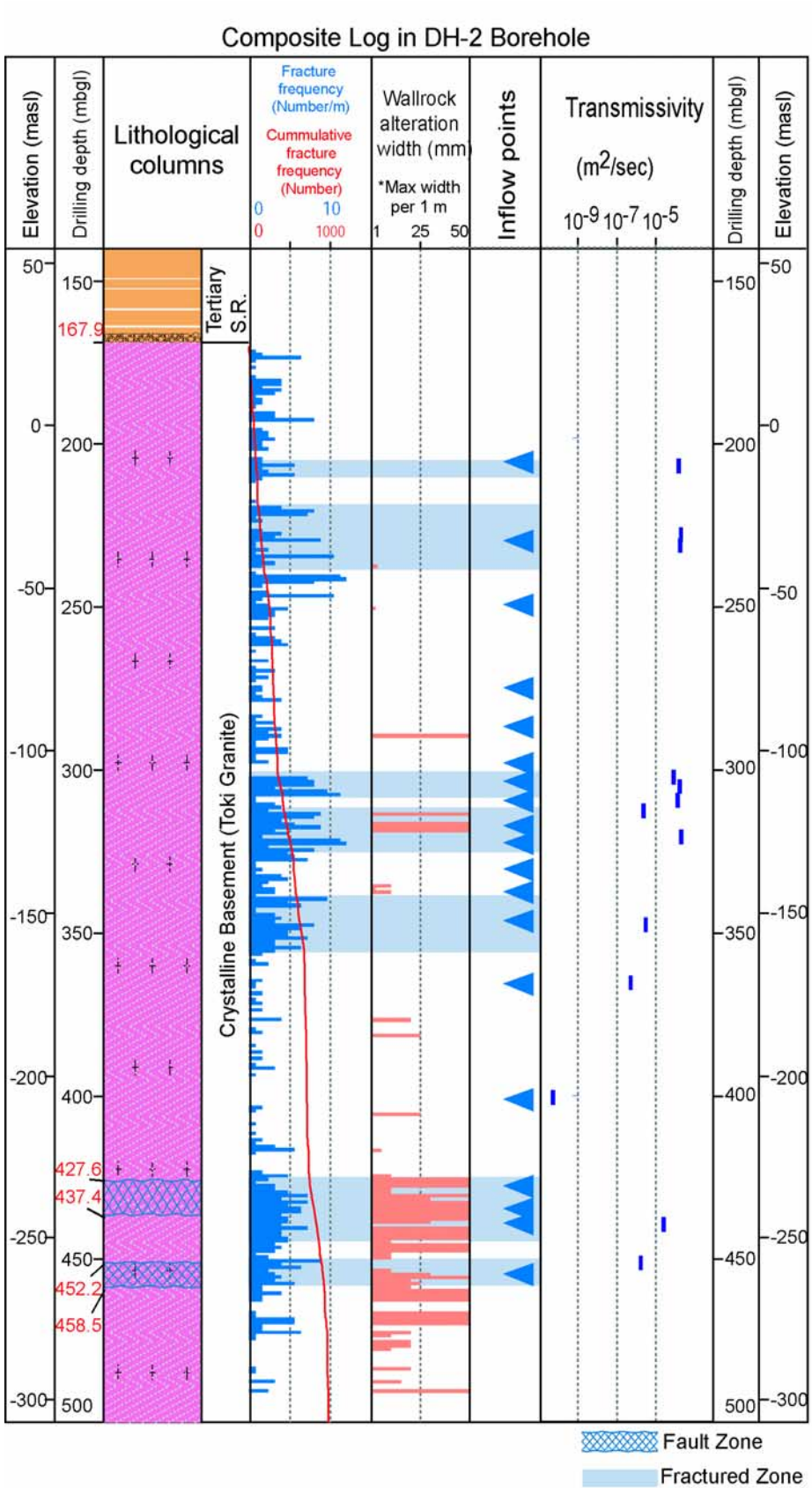

Figure 15. Overview of well DH-2 borehole investigations. The column labeled "inflow points" shows flowing FEC logging results. The length of the segment showing transmissivity identifies the distance between packers.

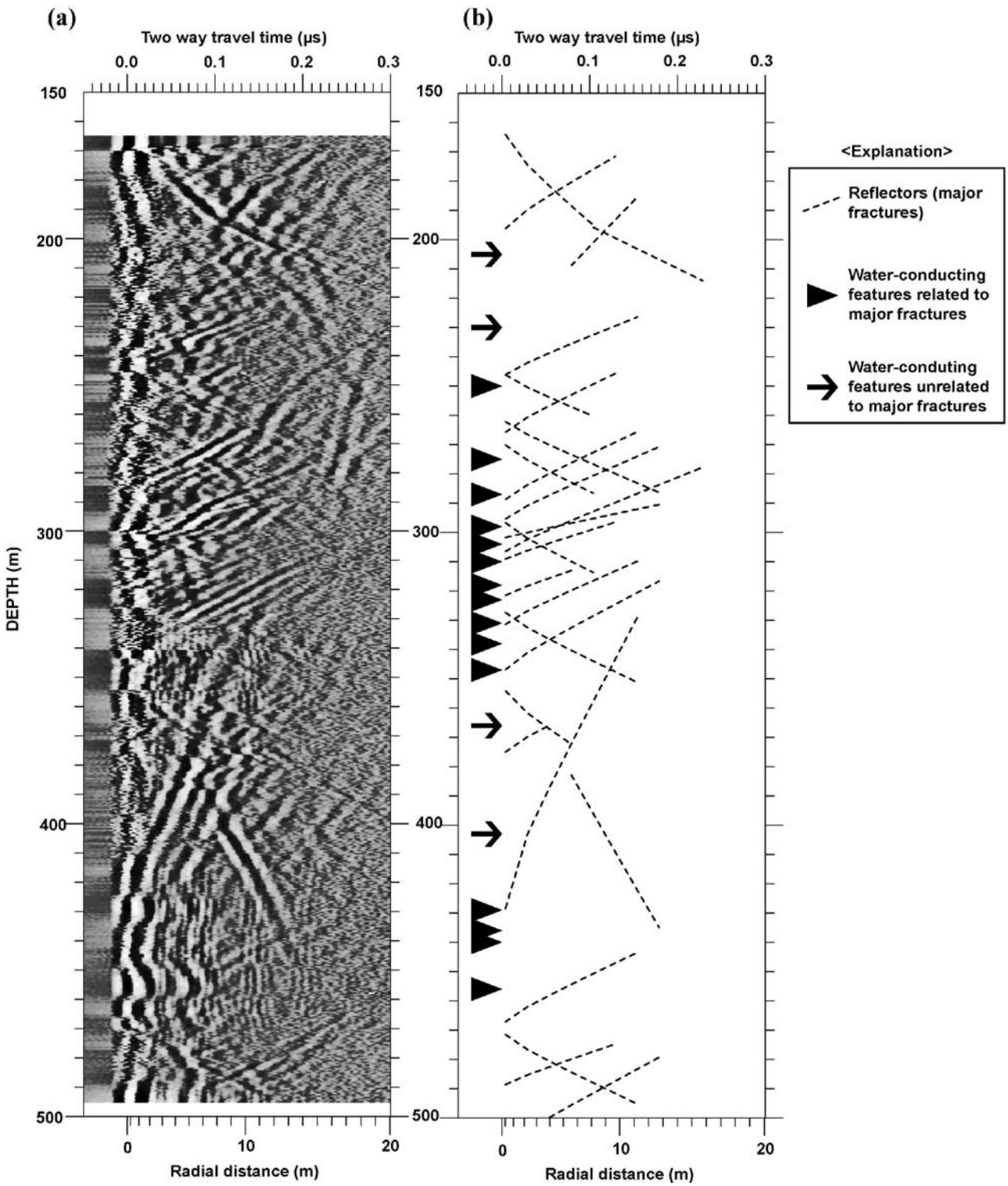

Figure 16. (a) Borehole radar log and (b) interpreted reflectors with the locations of water-conducting features identified by flowing FEC logging.

[57] The present analysis has successfully demonstrated the potential for the flowing FEC logging method as a hydrogeological characterization tool for fractured rock. On the basis of this experience, we can make several recommendations for future applications. First, although pressure head data are not needed for the main results (equations (1) and (4)), every effort should be made to obtain a valid measurement of the quiescent pressure in the well bore, P_{avg}. Given all the well bore activity accompanying flowing FEC logging, this may require adding or extending nonpumping periods within the field schedule. A second important pressure measurement is the well bore pressure drop during pumping, $(P_{avg} - P_{wb})$. If both P_{avg} and P_{wb} can be measured, then their difference is obtained automat-

Table A1. Field Logging Schedule

Activity Time		Measurement Time		
Start	End	Start	End	Description
				21 Aug
8:00	8:30			site preparation
8:30	12:00			install EC logging tools and tubing (tubing bottom at 493.8 m[a])
12:00	12:40			install pump and water level sensor (pump at 49.9 m, sensor at 45.9 m)
13:32	8:53[b]			replace well bore water with deionized water (CIRCULATION 1)
				22 Aug
8:55	9:15			remove pump
9:21	10:42			remove EC logging tools and tubing
		9:21	10:35	EC measurement (STATIC UP)
		10:49	11:25	EC measurement (STATIC DOWN)
11:40	12:00			install pump and water level sensor (pump at 50.2 m, sensor at 46.2 m)
12:09	19:25			PUMPING at Q = 10 L/min
		12:13	12:30	EC measurement (Q = 10 L/min, t = 0 hr DOWN)
		12:30	12:44	EC measurement (Q = 10 L/min, t = 0 hr UP)
		13:09	13:24	EC measurement (Q = 10 L/min, t = 1 hr DOWN)
		13:25	13:41	EC measurement (Q = 10 L/min, t = 1 hr UP)
		14:09	14:25	EC measurement (Q = 10 L/min, t = 2 hr DOWN)
		14:25	14:40	EC measurement (Q = 10 L/min, t = 2 hr UP)
		15:09	15:25	EC measurement (Q = 10 L/min, t = 3 hr DOWN)
		15:25	15:40	EC measurement (Q = 10 L/min, t = 3 hr UP)
		16:09	16:25	EC measurement (Q = 10 L/min, t = 4 hr DOWN)
		16:25	16:40	EC measurement (Q = 10 L/min, t = 4 hr UP)
		17:09	17:25	EC measurement (Q = 10 L/min, t = 5 hr DOWN)
		17:25	17:41	EC measurement (Q = 10 L/min, t = 5 hr UP)
		18:09	18:25	EC measurement (Q = 10 L/min, t = 6 hr DOWN)
		18:25	18:41	EC measurement (Q = 10 L/min, t = 6 hr UP)
19:25	19:45			remove pump
19:55	21:25			install EC logging tools and tubing (tubing bottom at 488.8 m)
21:25	22:00			install pump and water level sensor (pump at 50.2 m, sensor at 46.2 m)
22:17	8:34[b]			replace well bore water with deionized water (CIRCULATION 2)
				23 Aug
8:35	9:08			remove pump
9:08	9:58			remove EC logging tools and tubing
		9:09	9:56	EC measurement (STATIC UP)
		10:08	10:26	EC measurement (STATIC DOWN)
10:40	11:00			install pump and water level sensor (pump at 50.2 m, sensor at 46.2 m)
11:02	17:56			PUMPING at Q = 20 L/min
		11:09	11:25	EC measurement (Q = 20 L/min, t = 0 hr DOWN)
		11:25	11:42	EC measurement (Q = 20 L/min, t = 0 hr UP)
		12:02	17:35	repeat down and up measurements at one hour intervals for 6 hours
18:00	18:30			remove pump
18:30	19:30			install EC logging tools and tubing (tubing bottom at 488.8 m)
19:30	19:58			install pump and water level sensor (pump at 50.2 m, sensor at 46.2 m)
20:12	6:28[b]			replace well bore water with deionized water (CIRCULATION 3)
				24 Aug
6:30	6:45			remove pump
6:48	7:34			remove EC logging tools and tubing
		06:48	07:33	EC measurement (STATIC UP)
		07:43	08:00	EC measurement (STATIC DOWN)
8:17	8:32′			install pump and water level sensor (pump at 50.2 m, sensor at 46.2 m)
8:32	15:16			PUMPING at Q = 5 L/min
		08:35	08:51	EC measurement (Q = 5 L/min, t = 0 hr DOWN)
		08:52	09:10	EC measurement (Q = 5 L/min, t = 0 hr UP)
		09:32	15:15	repeat down and up measurements at one hour intervals for 6 hours

[a]Numbers refer to depth below the ground surface; water level in the well bore varied between 24.4 and 25.6 m during field operations.
[b]The next morning.

ically. However, if one or the other cannot be measured individually, knowledge of the difference is valuable in itself.

[58] Additionally, it is very important to be able to judge whether the assumption that $\Sigma q_i = Q$ is reasonable. When choosing q_i by trial and error, the constraint that $\Sigma q_i = Q$ greatly expedites the process, but it has been noted at other field sites that large contributions to Q can come from zones beyond the range of FEC logging, invalidating the assumption. For the test 3 profiles, the evenly spaced FEC fronts enable fluid velocity up the well bore to be determined, which in conjunction with well bore diameter, provides an independent measure of Q, supporting the assumption that $\Sigma q_i = Q$.

[59] Finally, analysis of the DH-2 data, with its significant internal flow under nonpumping conditions, has made obvious the need for a better means of assigning initial conditions for BORE II. For cases in which internal flow is small or absent, static profiles will be nearly uniform in space and time with small or zero FEC, and will provide suitable initial conditions for BORE II. However, when internal flow is significant, both "static" ($Q = 0$) and flowing ($Q \neq 0$) profiles change with time. Since the probe takes a finite amount of time to complete a profile, using any measured FEC profile as an initial condition is problematic in that the time dependence of the profile is lost. The successful static profile analysis presented in section 5.2 suggests that after a preliminary multirate analysis using flowing FEC logs is done, it may be feasible to do a longer BORE II simulation including both the static and pumping periods. Such a combined simulation would use a uniform or nearly uniform initial condition (e.g., Figure 14 dotted line) and match all the static and flowing FEC profiles, instead of assuming any of them as initial conditions.

Appendix A

[60] The complete field logging schedule for the three sets of FEC logs obtained at different pumping rates is shown in Table A1.

[61] **Acknowledgments.** The reviews of this paper by Barry Freifeld and Curt Oldenburg of Lawrence Berkeley National Laboratory and by two anonymous reviewers and the Associate Editor of *Water Resources Research* are greatly appreciated. We thank the Geophysical Surveying Company, Ltd., Japan, and, in particular, Kiyoyuki Matsuoka for conducting the field logging operations. This work was jointly supported by the Director, Office of Science, Office of Basic Energy Sciences, Geoscience Program of the U.S. Department of Energy, the Taisei Corporation of Japan, and Japan Nuclear Cycle Development Institute (JNC) under the Binational Research Cooperative Program between JNC and U.S. Department of Energy, Office of Environmental Management, Office of Science and Technology (EM-50). The work was performed under contract DE-AC03-76SF00098.

References

Bauer, G. D., and J. J. LoCoco (1996), Hydrogeophysics determines aquifer characteristics, *Int. Ground Water Technol.*, *2*, 12–16.

Brainerd, R. J., and G. A. Robbins (2004), A tracer dilution method for fracture characterization in bedrock wells, *Ground Water*, *42*(5), 774–780.

Cooper, H. H., and C. E. Jacob (1946), A generalized graphical method for evaluating formation constants and summarizing well field history, *Eos Trans. AGU*, *27*, 526–534.

Doughty, C., and C.-F. Tsang (2000), BORE II—A code to compute dynamic wellbore electrical conductivity logs with multiple inflow/outflow points including the effects of horizontal flow across the well, *Rep. LBL-46833*, Lawrence Berkeley Natl. Lab., Berkeley, Calif.

Doughty, C., and C.-F. Tsang (2005), Signatures in flowing fluid electric conductivity logs, *J. Hydrology*, *310*(1–4), 157–180.

Drost, W., D. Klotz, A. Koch, H. Moser, F. Neumaier, and W. Rauert (1968), Point dilution methods of investigating ground water flow by means of radioisotopes, *Water Resour. Res.*, *4*(1), 125–146.

Evans, D. G. (1995), Inverting fluid conductivity logs for fracture inflow parameters, *Water Resour. Res.*, *31*(12), 2905–2915.

Evans, D. G., W. P. Anderson Jr., and C.-F. Tsang (1992), Borehole fluid experiments near salt contamination sites in Maine, paper presented at Conference on Eastern Regional Ground Water Issues, Natl. Ground Water Assoc., Newton, Mass.

Guyonnet, D., A. Rivera, S. Löw, and N. Correa (1993), Analysis and synthesis of fluid logging data from Wellenberg boreholes SB1, SB3, SB4 and SB6, *Tech. Rep. NTB 92-01*, 153 pp., Nagra, Wettington, Switzerland.

Hale, F. V. and C.-F. Tsang (1988), A code to compute borehole conductivity profiles from multiple feed points, *Rep. LBL-24928*, Lawrence Berkeley Natl. Lab., Berkeley, Calif.

Karasaki, K., B. Freifeld, A. Cohen, K. Grossenbacher, P. Cook, and D. Vasco (2000), A multidisciplinary fractured rock characterization study at Raymond field site, Raymond, CA, *J. Hydrol.*, *236*, 17–34.

Kelley, V. A., J. M. Lavanchy, and S. Löw (1991), Transmissivities and heads derived from detailed analysis of Siblingen 1989 fluid logging data, *Tech. Rep. NTB 90-09*, 184 pp., Nagra, Wettington, Switzerland.

Löw, S., V. Kelley, and S. Vomvoris (1994), Hydraulic borehole characterization through the application of moment methods to fluid conductivity logs, *J. Appl. Geophys.*, *31*(1–4), 117–131.

Marschall, P., and S. Vomvoris (Eds.) (1995), Grimsel Test Site: Developments in hydrotesting, fluid logging and combined salt/heat tracer experiments in the BK Site (Phase III), *Tech. Rep.93-47*, Nagra, Wettington, Switzerland.

National Research Council (1996), *Rock Fractures and Fluid Flow: Contemporary Understanding and Applications*, Natl. Acad. Press, Washington, D. C.

Öhberg, A., and P. Rouhiainen (2000), Groundwater flow measuring techniques, *Rep. Posiva 2000-12*, Posiva Oy, Helsinki.

Paillet, F. L., and W. H. Pedler (1996), Integrated borehole logging methods for wellhead protection applications, *Eng. Geol.*, *42*(2–3), 155–165.

Pedler, W. H., C. L. Head, and L. L. Williams (1992), Hydrophysical logging: A new wellbore technology for hydrogeologic and contaminant characterization of aquifers, paper presented at National Outdoor Action Conference, Natl. Ground Water Assoc., Las Vegas, Nevada.

Schlumberger, Ltd. (1984), *Log Interpretation Charts*, New York.

Tsang, C.-F., and C. Doughty (2003), Multirate flowing fluid electric conductivity logging method, *Water Resour. Res.*, *39*(12), 1354, doi:10.1029/2003WR002308.

Tsang, C.-F., P. Hufschmeid, and F. V. Hale (1990), Determination of fracture inflow parameters with a borehole fluid conductivity logging method, *Water Resour. Res.*, *26*(4), 561–578.

C. Doughty and C.-F. Tsang, Earth Sciences Division, Lawrence Berkeley National Laboratory, 1 Cyclotron Road, MS 90-1116, Berkeley, CA 94720, USA. (cadoughty@lbl.gov)

K. Amano and S. Takeuchi, Mizunami Underground Research Laboratory, Tono Geoscience Center, Japan Nuclear Cycle Development Institute, 1-64, Yamanouchi, Akeyo-cho, Mizunami-shi Gifu, 509-6132, Japan.

M. Shimo, Civil Engineering Research Institute, Technology Center, Taisei Corporation, 344-1, Nase-cho, Totsuka-ku, Yokohama, Kanagawa, 245-0051, Japan.